ACS OMEGA

Open Access

This article is licensed under CC-BY-NC-ND 4.0

http://pubs.acs.org/journal/acsodf

Article

Water-Induced Turn-on of Lanthanide Photoluminescence Emission and Application in Colorimetric Sensing of Trace Water

Malee Sinchow, Rania Chaicharoen, Thammanoon Chuasaard, Bunlawee Yotnoi, Chalermpong Saenjum, Athipong Ngamjarurojana, and Apinpus Rujiwatra*

Cite This: *ACS Omega* 2024, 9, 49441−49451

Read Online

ACCESS | Metrics & More | Article Recommendations | Supporting Information

ABSTRACT: To examine the water-induced photoluminescence turn-on and its potential application in trace water sensing, a new series of $[Ln^{III}(dmba)_3(H_2O)_2]\cdot 2H_2O$, where Ln^{III} = La^{III} (**I**), Pr^{III} (**II**), Nd^{III} (**III**), Sm^{III} (**IV**), Eu^{III} (**V**), Gd^{III} (**VI**), Tb^{III} (**VII**), Dy^{III} (**VIII**), Ho^{III} (**IX**), and Er^{III} (**X**), were synthesized using dimethoxybenzoic acid (Hdmba). Their single-crystal structures and thermal and chemical robustness were investigated, and the effects of lanthanide contraction and noncovalent interactions were discussed. The photoluminescence and colorimetric properties of **I**−**X** were investigated. Their dependence on dehydration and rehydration was disclosed, from which the significant role of noncovalent interactions was proposed. Based on the dehydration−rehydration-dependent responses in the forms of photoluminescence emission and color, the turn-off (dehydration) and turn-on (rehydration) of the red emission of Eu^{III} (**V**) were demonstrated. Using a mobile phone camera and freeware application, its use in the colorimetric sensing of trace water in polar organic solvents was successfully achieved. With respect to ethanol, acetonitrile, and acetone, linear correlations were established from 0 to 3−5% by volume of water with an R^2 of over 0.98. The detection and quantification limits were less than 0.5 and 1.5%, respectively. The percentage recoveries were 92 and 110%. The underlying mechanism was postulated.

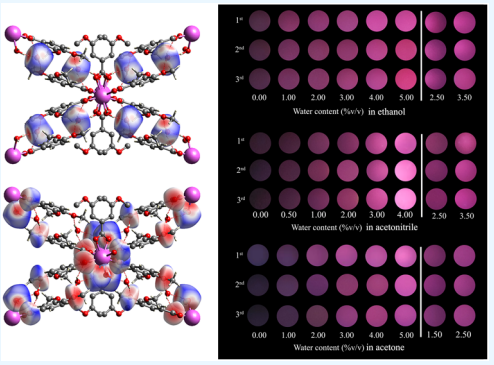

1. INTRODUCTION

Water is considered as a contaminant regarding organic solvents used in various industrial processes.[1,2] To determine trace water in these organic solvents, several conventional methods are available, such as Karl Fischer titration, gas chromatography, and electrical measurements.[1,2] These techniques generally require expensive instruments and skillful handling. The search for alternative methods, which are simpler, inexpensive, and less skill-demanding, has been actively ongoing, particularly those based on photophysical properties.[3] This is because techniques based on photophysical properties are generally noninvasive, simple to operate, fast-responsive, and highly sensitive.[1,2] In line with this, lanthanide coordination polymers (Ln^{III}-CPs) possessing an exceptional affinity for water and unique photophysical properties[4−6] are promising candidates, although several issues still need to be overcome.[7,8]

Coordination polymers (CPs) are coordination compounds containing indefinite one-, two-, or three-dimensional framework structures that are constructed from two basic structural building motifs, i.e., inorganic coordination moieties as nodes and organic ligands as linkers. They are well recognized for their potential applications, for instance, in biomedical imaging,[9,10] light-emitting devices,[11,12] sensing,[13] and catalysis.[14−18] When the coordination moieties are made up of lanthanides, which commonly exist in the trivalent state (Ln^{III}), Ln^{III}-CPs are formed. In view of crystal engineering, it is a challenge to synergize the advantageous features of both CPs and Ln^{III}.[19−21] One of the available strategies is through the use of appropriate organic ligands, which are crucial in regulating both the framework structure and photophysical properties of the included Ln^{III}.[7,8] Because of the hard acidic nature of Ln^{III}, viable organic ligands are notably limited to mostly aromatic polycarboxylates.[22] Modifying the molecular structures of these organic ligands appears as an alternative approach to diversify the structure and properties of the derived Ln^{III}-CPs. For example, the use of 2-amino-1,4-benzenedicarboxylic acid ($H_2bdc\text{-}NH_2$) led to $[Eu_2(bdc\text{-}NH_2)_3(DMF)_4]\cdot 2DMF$[23] of which the photoluminescence property differed from Eu-bdc-OH constructed using 2-hydroxy-1,4-benzenedicarboxylic acid ($H_2bdc\text{-}OH$).[24]

With respect to water sensing applications, the presence of water in the framework structures of Ln^{III}-CPs commonly leads

Received: July 29, 2024
Revised: October 12, 2024
Accepted: November 27, 2024
Published: December 2, 2024

© 2024 The Authors. Published by American Chemical Society

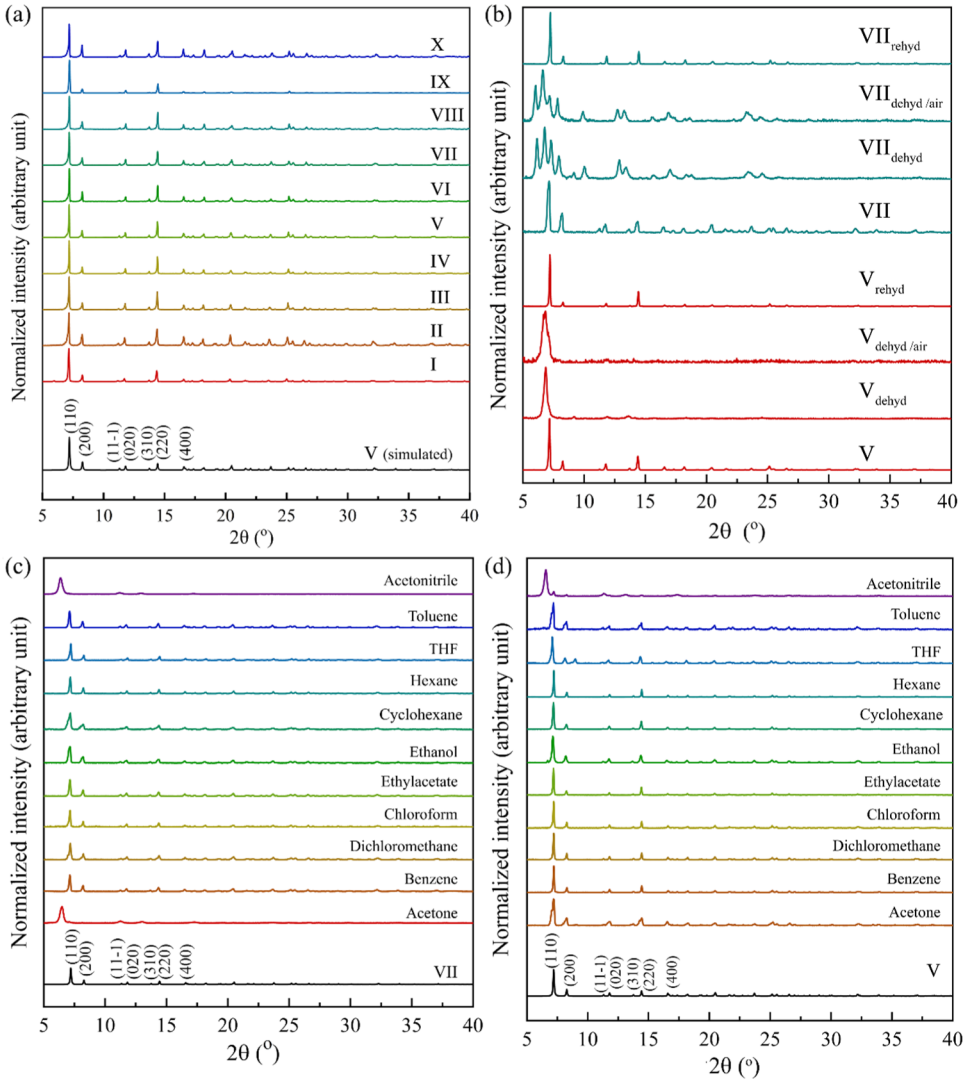

Figure 1. PXRD patterns of (a) the as-synthesized **I**–**X** compared with the pattern simulated from the single-crystal data of **V** (as a representative of **I**–**X**), (b) dehydrated ($\mathbf{V}_{dehyd}$, $\mathbf{VII}_{dehyd}$) and rehydrated ($\mathbf{V}_{rehyd}$ and $\mathbf{VII}_{rehyd}$) samples, and (c) **V** and (d) **VII** after soaking in different solvents for 24 h.

to nonradiative decay and is detrimental to both antenna-centered intersystem crossing and antenna-to-Ln^{III} energy transfer.[7,8] Both processes are important in promoting photoluminescence emissions of Ln^{III}-CPs according to the antenna model.[7,8] Therefore, the application of Ln^{III}-CPs in water-containing systems is generally impracticable[25] although there have been few reports on water-induced enhancement of photoluminescence emission. Some previously reported examples are Eu^{III}-dibenzoylmethane,[26] QXBA-Eu-1 and QXBA-Eu-2,[27] and Eu^{III}-*p*-fluorobenzoate.[8] Their use in sensing trace water in organic solvents has been demonstrated.[8,26−28]

Aiming at the water-induced emission enhancement and therefore the water sensing applications, a new series of $[Ln^{III}(dmba)_3(H_2O)_2]\cdot 2H_2O$, where Ln^{III} = La^{III} (**I**), Pr^{III} (**II**), Nd^{III} (**III**), Sm^{III} (**IV**), Eu^{III} (**V**), Gd^{III} (**VI**), Tb^{III} (**VII**), Dy^{III} (**VIII**), Ho^{III} (**IX**), and Er^{III} (**X**), were synthesized. Hdmba was selected because of its sensitizing ability.[29] In addition, it is a small molecule that should allow the coordination of water molecules to Ln^{III} and thus match the objective of this research. The crystal structures of **I**–**X** were elucidated and analyzed. Their thermal and chemical stabilities, as well as their photophysical properties, were studied. The dependence of photoluminescence and colorimetric properties of **V** and **VII** on dehydration and rehydration was explored from which the water-induced photoluminescence enhancement of **V** was revealed. The potential of **V** as a colorimetric probe for visible detection and determination of trace water in organic solvents was then evaluated using a mobile phone camera and a freeware application.

2. EXPERIMENTAL SECTION

Details on the materials, instruments, characterization methods, and single-crystal structure determination[30−33] are provided in the Supporting Information.

2.1. Synthesis and Crystal Growth of I–X. As a general procedure, an aqueous solution of $Ln(NO_3)_3\cdot 6H_2O$ (0.200 mmol), Hdmba (0.200 mmol), and triethylamine (40.0 μL) was prepared in a 15.00 mL glass vial using 10.00 mL of deionized water. After stirring at room temperature for 10 min, tiny crystals of the corresponding product were obtained. The weights of the reagents and yields of the products are listed in Table S1. Alternatively, large single crystals appropriate for

https://doi.org/10.1021/acsomega.4c06958
ACS Omega 2024, 9, 49441−49451

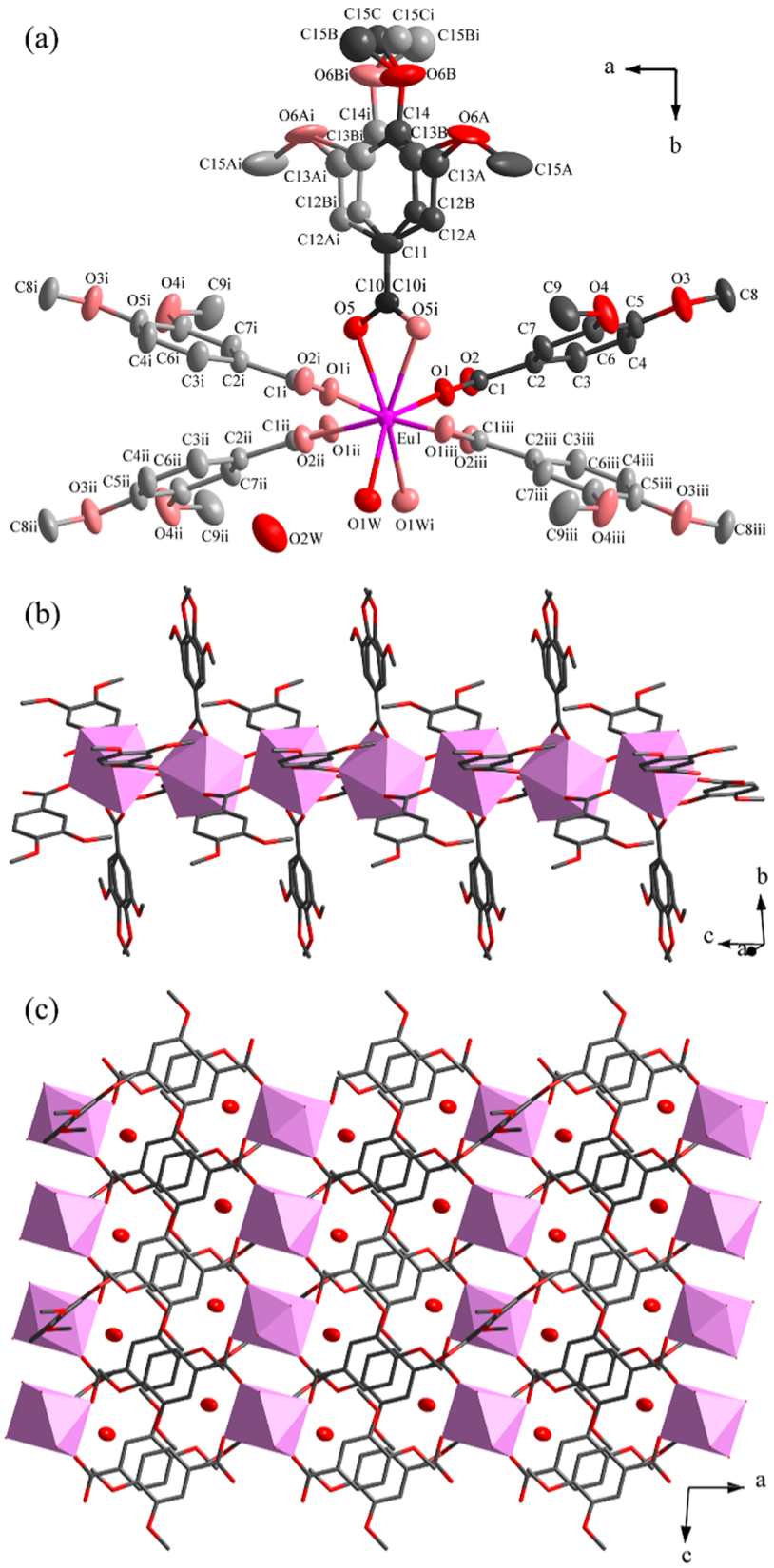

Figure 2. Views of (a) an extended asymmetric unit of **V** (Eu^{III}) drawn using 50% probability for ellipsoids, (b) a one-dimensional chain, and (c) a three-dimensional assembly (H atoms have been omitted for clarity). Symmetry operations: (i) $1 - x, y, 0.5 - z$, (ii) $1 - x, 1 - y, 1 - z$, and (iii) $x, 1 - y, -0.5 + z$.

single-crystal X-ray diffraction experiments can be obtained from the reactions performed at 60 °C for 24 h.

2.2. Photoluminescence and Colorimetric Measurements. The photoluminescence spectra of the solid samples

https://doi.org/10.1021/acsomega.4c06958
ACS Omega 2024, 9, 49441−49451

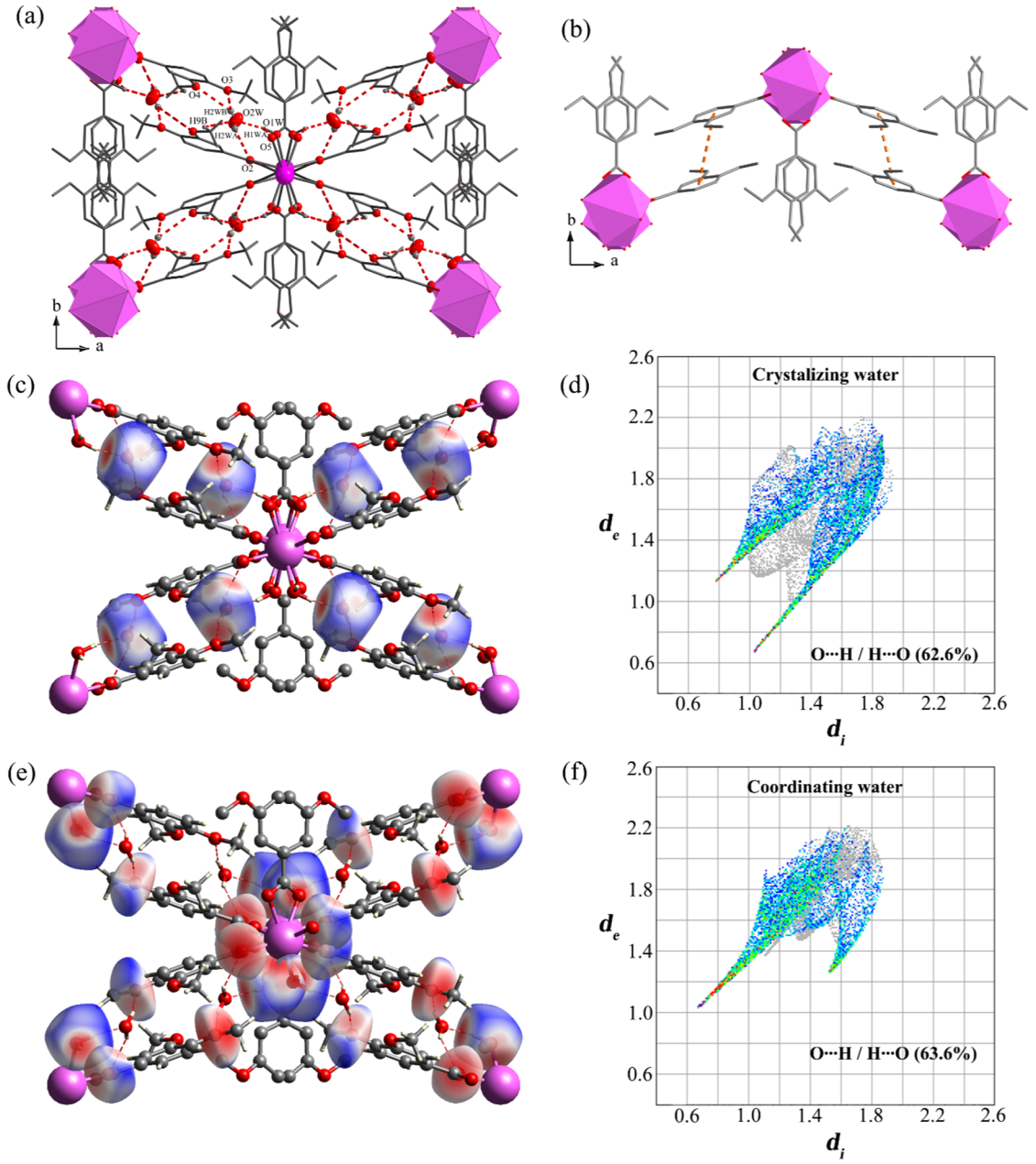

Figure 3. Depictions of (a) hydrogen bonding and (b) aromatic $\pi-\pi$ interactions in **V** (as a representative of **I**–**X**), (c) the three-dimensional Hirshfeld surface of the crystallizing water molecules, (d) the corresponding two-dimensional fingerprint plot, and (e) the Hirshfeld surface of the framework's O atoms with (f) the corresponding fingerprint plot.

and their suspensions in different solvents were collected at room temperature using an ASEQ LR-1T broad-range spectrophotometer equipped with an ultrafine G60 LED flashlight torch (5 W, 365 nm) and a UV optical band-pass (400 nm). To eliminate any interference from ambient light, the entire setup was installed in a black chamber. The colors of the emissions were captured in JPEG format using a smartphone camera (Samsung A71, aperture F1.8, ISO2500, speed shutter 1/10 s) installed in the black chamber. For the solid samples, the camera was fixed at ca. 45° and 5 cm from the center of the sample holder. For the suspensions, the camera was installed at the same level as the cuvette holder and 25 cm from the holder. The captured photographs were analyzed in the RGB colorimetric space using the Color Picker application.[34] The emission lifetimes were measured by using a JASCO FP-8500 fluorescence spectrometer. The excitation wavelength was set to 370 nm, whereas the observation wavelengths were fixed at 618 nm for Eu^{III} and 545 nm for Tb^{III}.

2.3. Trace Water Sensing Experiments. The photoluminescence spectra and colors of suspensions of dehydrated **V** or $\mathbf{V}_{dehyd}$ (10.0 mg) in dried organic solvents (3.00 mL) were studied using excitation at 365 nm. $\mathbf{V}_{dehyd}$ was prepared by heating finely ground **V** at 120 °C for 30 min. The tested solvents were ethanol (C_2H_5OH), acetonitrile (CH_2CN), acetone ($(CH_3)_2CO$), ethyl acetate ($CH_3CO_2C_2H_5$), tetrahydrofuran ($(CH_2)_4O$, THF), dichloromethane (CH_2Cl_2), chloroform ($CHCl_3$), benzene (C_6H_6), toluene ($C_6H_5CH_3$), cyclohexane (C_6H_{12}), and hexane (C_6H_{14}). Following the procedure suggested in the literature,[35] the samples were dried

https://doi.org/10.1021/acsomega.4c06958
ACS Omega 2024, 9, 49441−49451

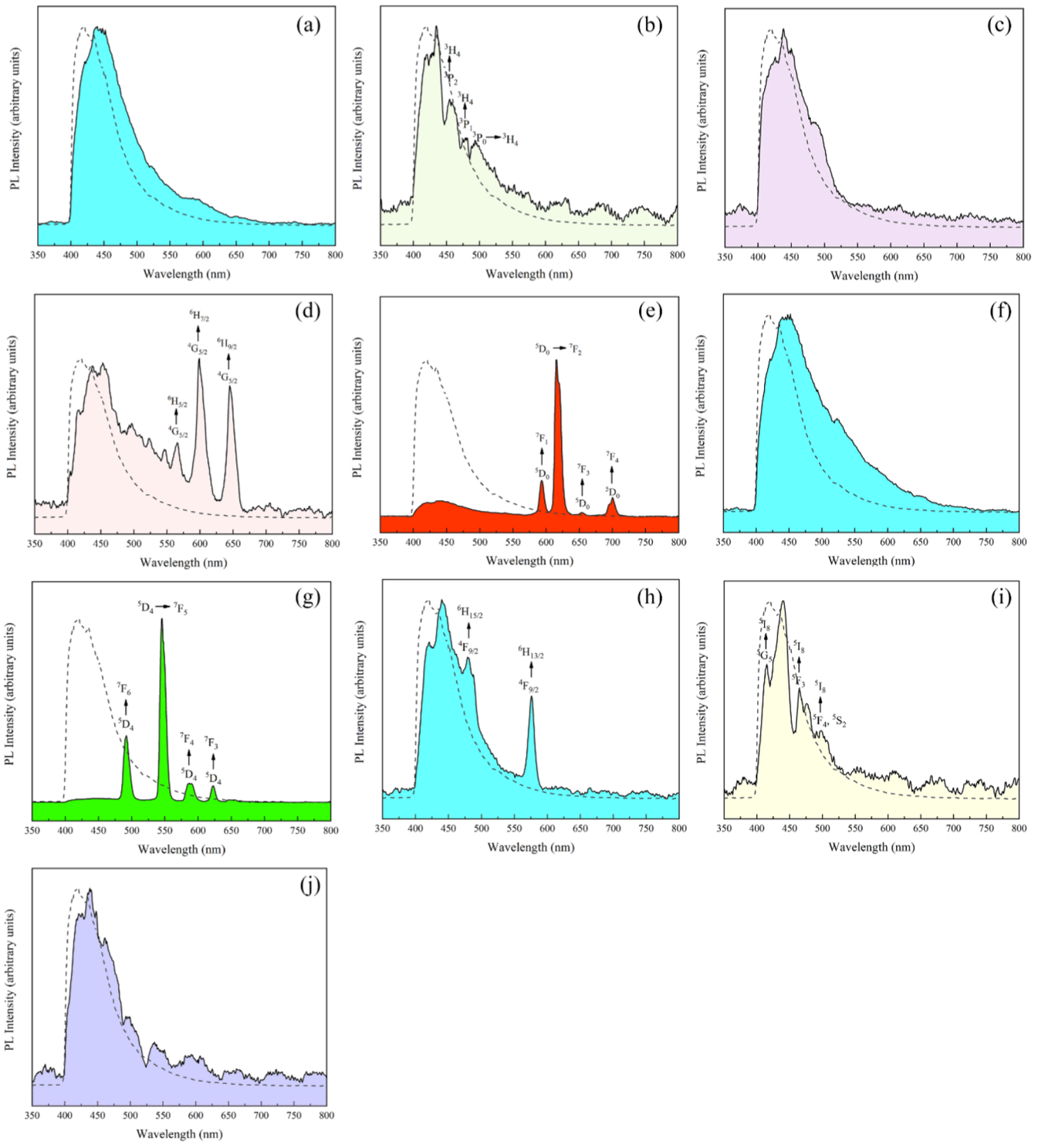

Figure 4. Solid-state emission spectra (solid line) of (a) **I** (La^{III}), (b) **II** (Pr^{III}), (c) **III** (Nd^{III}), (d) **IV** (Sm^{III}), (e) **V** (Eu^{III}), (f) **VI** (Gd^{III}), (g) **VII** (Tb^{III}), (h) **VIII** (Dy^{III}), (i) **IX** (Ho^{III}), and (j) **X** (Er^{III}) compared with that of Hdmba (dotted line).

using molecular sieves (Aldrich Chemical Co. Ltd., 5 Å, beads, 8−12 mesh) before use. To evaluate the water sensing performance, the water content of these solvents was varied from 0% (dried solvents) to 5% by volume (%v/v). For ethanol, the water contents were verified by Karl Fisher titration (V20 Compact Volumetric KF Titrator, METTLER TOLEDO). Reuse experiments were conducted by using ethanol as a representative solvent. $\mathbf{V}_{dehyd}$ was recovered by filtration and then dried at 120 °C for 30 min.

3. RESULTS AND DISCUSSION

3.1. Synthesis and Crystal Structure Description.

According to single-crystal data (Table S2 and Figure S1), **I**−**X** are isostructural and can be solved and refined in the monoclinic *C*2/*c* space group. The refined unit cell parameters (except *a*) show a decreasing tendency from **I** to **X** (Figure S2), which corresponds to lanthanide contraction. PXRD experiments (Figure 1) were used to confirm the purity.

https://doi.org/10.1021/acsomega.4c06958
ACS Omega 2024, 9, 49441−49451

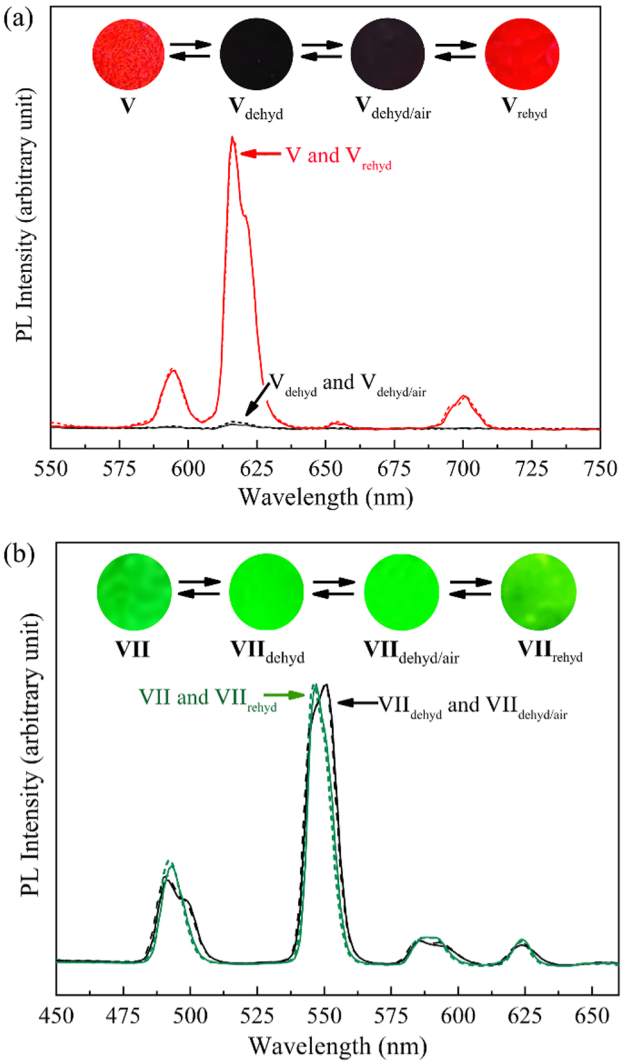

Figure 5. Emission spectra and colors of the emissions observed from the as-synthesized, dehydrated ($\mathbf{V}_{dehyd}$ and $\mathbf{V}_{rehyd}$), air-exposed dehydrated ($\mathbf{V}_{dehyd/air}$ and $\mathbf{VII}_{dehyd/air}$), and rehydrated ($\mathbf{VII}_{dehyd}$ and $\mathbf{VII}_{rehyd}$) samples (a) **V** and (b) **VII**.

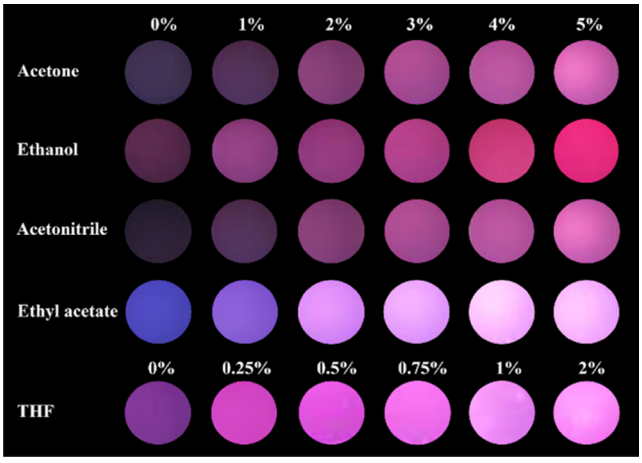

Figure 6. Photographs showing a gradual change in the emission colors captured from the suspensions of $\mathbf{V}_{dehyd}$ in various polar solvents (under excitation at 365 nm and a contact time of 40 s).

Notably, these pure phases can be easily and rapidly prepared in high yields as tiny crystals after mixing and stirring under ambient conditions for 10 min. This is considered beneficial for upscaling. Alternatively, large crystals could be produced by carrying out the synthesis at 60 °C for 24 h.

The crystal structures of **I**–**X** are supramolecular assemblies of the one-dimensional $[Ln^{III}(dmba)_3(H_2O)_2]$ chain extending in the *c* direction (Figures 2 and S3). The chain is constructed based on one crystallographically unique Ln^{III}, which is 8-fold-coordinated to eight O atoms from one chelating $dmba^-$, four monodentate $dmba^-$, and two water molecules (Figure S1). Chelating $dmba^-$ shows disorder over two crystallographic sites with approximately equal site occupancy. The eight donor atoms define a distorted triangular dodecahedral geometry and, therefore, the *DD*-$\{Ln^{III}\text{-}O_8\}$ structural building motif. Through the four −OCO− bridges of four monodentate $dmba^-$, each *DD*-$\{Ln^{III}\text{-}O_8\}$ is linked to two neighboring equivalents to form a one-dimensional chain. In the *b* direction, the chain is decorated with chelating $dmba^-$ and coordinating water molecules. In the *ac* plane, monodentate $dmba^-$ resides. These chains are assembled via these dangling motifs. In the direction of *a*, the assembly can be viewed as an alternative interlocking between inorganic and organic arrays. This interlocking may be the reason for the independence of the *a* parameter from lanthanide contraction (Figure S2a).

The assembly of the one-dimensional chains is stabilized through O−H···O and C−H···O hydrogen bonding as well as aromatic π−π interactions (Figure 3 and Tables S3−S12). The continual increase in the centroid-to-centroid distances of the π−π interactions from 4.243 Å in **I** to 4.337 Å in **X** is also in good accordance with lanthanide contraction. The smaller Ln^{III} centers result in longer distances between the interacting aromatic rings. There is a small void within the chain assembly where the crystallizing water molecules are housed. They are transfixed to the framework through hydrogen bonding interactions. Their interactions with the methoxy group of $dmba^-$ may be attributed to site disordering of this ligand. The calculation using PLATON[36] suggests, nonetheless, a negligible void space with an insignificant void opening through which only water can pass. This reflects the molecular sieve properties of **I**–**X**.

To visualize the hydrogen bonding interactions, a three-dimensional Hirshfeld surface analysis of **V** (as a representative of **I**–**X**) was carried out (Figure 3).[37,38] Red surfaces appeared close to both the coordinating and crystallizing water as well as the methoxy groups, indicating the close contacts of these structural moieties. These results are in excellent agreement with the O−H···O and C−H···O hydrogen bonding interactions listed in Table S7. The corresponding two-dimensional fingerprint plots acquired from the Hirshfeld surfaces emphasize the significance of O−H···O interactions. The pair of spikes at the bottom left of the plots is characteristic of the strong O···H contacts. The reciprocal O···H contacts are displayed in the blue and turquoise regions of the plots and account for over 60% of entire interactions involved with the analyzed atoms. The substantial involvement of these structural moieties in hydrogen bonding interactions is therefore affirmed.

The complete matching between the PXRD patterns simulated from the single-crystal data and those of the as-synthesized samples (Figure 1) indicates that the crystals are good representatives of the yielded samples. Elemental analysis provided consistent results (Table S1), and the expected

https://doi.org/10.1021/acsomega.4c06958
ACS Omega 2024, 9, 49441−49451

Table 1. Performance of V_{dehyd} as a Colorimetric Sensing Probe for Determining Trace Water Compared with the Other Previously Reported Probes

probe	solvent	used parameter	linear range (%v/v)	LOD (%v/v)	LOQ (%v/v)	response time	ref
V_{dehyd}	ethanol	R	0.00−5.00	0.147	0.491	40 s	this work
		B	0.00−4.00	0.375	1.25		
		L	0.00−5.00	0.476	1.59		
	acetonitrile	R	0.00−5.00	0.402	1.34	40 s	
		B	0.00−5.00	0.216	0.719		
		L	0.00−4.00	0.320	1.07		
	acetone	R	0.00−4.00	0.195	0.650	40 s	
		B	0.00−3.00	0.299	0.995		
		L	0.00−3.00	0.00103	0.00345		
$Eu_{2.2}Tb_{97.8}$-TCA	ethanol	G/R[a]	0−0.67	0.035	NA	20 s	34
$Eu_{0.2}Tb_{0.8}$-UL	ethanol	G/R[a]	0−100	0.01	NA	20 min	45
TPA-2QA-OH	ethanol	R	0.02−0.20	0.0014	NA	NA	46
CDs@HKUST-1	EtOH	B	0−12	1.60	NA	45 min	47
	acetone	B	0−16	2.44	NA	45 min	
	acetonitrile	B	2−16	2.52	NA	45 min	

[a]Green-to-red ratio.

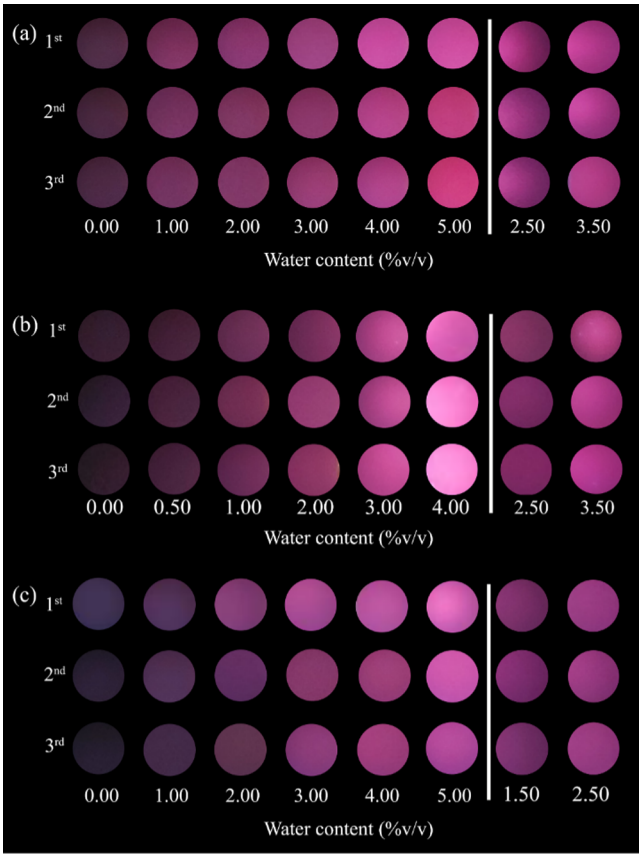

Figure 7. Photographs showing the captured emission colors used for the construction of calibration plots and those of the standard solvent samples containing specific water contents: (a) ethanol, (b) acetonitrile, and (c) acetone.

functional groups were observed in the FT-IR spectra (Figure S4 and Table S13).

3.2. Thermal Robustness of V and VII. Using thermogravimetric/differential thermal analysis (TG/DTA), the thermal stabilities of **V** and **VII** (representatives of **I**−**X**) were examined. Upon heating under nitrogen gas flow, two major weight losses occurred in both samples (Figure S5). The first loss with an onset at ca. 120 °C corresponds well with the removal of water molecules, whereas the second drastic loss at ca. 300 °C is attributed to the decomposition of the organic ligands and, therefore, the frameworks.

The plateau following the first weight loss implies the stability of both **V** and **VII** after the complete removal of water, i.e., dehydration. The PXRD patterns of **V** and **VII** reveal, however, different results (Figure S6). The heating of **V** led to the broadening and splitting of the most intense (110) peak. This change became more vivid with increasing temperatures above 120 °C. An entirely different PXRD pattern was then observed at 300 °C, from which a considerable change in its structure can be assumed. Interestingly, heating of **VII** at a lower temperature of 120 °C led to this considerable change.

As heating at 120 °C corresponds to dehydration (Figure S5), it can be concluded that heating at 120 °C for 30 min could provide the dehydrated $\mathbf{V}_{dehyd}$ and $\mathbf{VII}_{dehyd}$ (Figure 1), and **V** is structurally more robust against dehydration than **VII**. Compared with $\mathbf{V}_{dehyd}$, it may be assumed that the smaller Tb^{III} (**VII**) is more susceptible to structural changes than the larger Eu^{III} (**V**). This tendency was revealed by the change in the PXRD patterns of $\mathbf{I}_{dehyd}$ and $\mathbf{V}_{dehyd}$−$\mathbf{VIII}_{dehyd}$ prepared using the same thermal treatment conditions (Figure S8). The FT-IR spectra of both $\mathbf{V}_{dehyd}$ and $\mathbf{VII}_{dehyd}$ (Figure S7 and Table S14) confirmed the yield of the dehydrated phases. The characteristic vibrations of the water disappeared. The TG/DTA experiment on $\mathbf{V}_{dehyd}$ showed the absence of the dehydration step, additionally confirming this conclusion (Figure S9).

3.3. Reversible Dehydration and Rehydration of V and VII. The PXRD experiments (Figure 1) revealed that $\mathbf{V}_{dehyd}$ and $\mathbf{VII}_{dehyd}$ could be recovered to their original **V** and **VII**, respectively, under ambient conditions. This can be rationalized by the gradual resorption of atmospheric water. The process occurred, however, very slowly and could be accelerated by soaking the samples in water. Only 15 min could restore their PXRD (Figure 1), FT-IR (Figure S7), and TG/DTA (Figure S9) patterns to the original. Taking **V** as a representative of **V** and **VII**, its weights after dehydration and successive rehydration were monitored (Table S15). Based on three repetitions, the lost and gained weights were approximately identical and in good agreement with the TG/DTA experiments (Figure S9) and the $[Ln^{III}(dmba)_3(H_2O)_2]\cdot 2H_2O$

https://doi.org/10.1021/acsomega.4c06958
ACS Omega 2024, 9, 49441−49451

Table 2. Water Contents (%v/v) Determined in Standard Ethanol Samples Obtained Using V and Karl Fischer Titration

	values obtained using V_{dehyd} (%recovery)			
expected water content	R	B	L	values obtained from Karl Fischer titration (%recovery)
Ethanol				
			First Cycle	
2.50	2.47 ± 0.04 (99%)	2.54 ± 0.15 (102%)	2.31 ± 0.01 (92%)	2.34 ± 0.02 (94%)
3.50	3.61 ± 0.04 (103%)	3.52 ± 0.14 (100%)	3.46 ± 0.12 (99%)	3.32 ± 0.01 (95%)
			Second Cycle	
3.50	3.21 (92%)	3.47 (99%)	3.86 (110%)	
			Third Cycle	
3.50	3.21 (92%)	3.60 (103%)	3.86 (110%)	
			Fourth Cycle	
3.50	3.65 (104%)	3.34 (95%)	3.55 (102%)	
			Fifth Cycle	
3.50	3.21 (92%)	3.60 (104%)	3.24 (93%)	
Acetonitrile				
2.50	2.55 ± 0.06 (102%)	2.48 ± 0.04 (99%)	2.48 ± 0.01 (99%)	
3.50	3.60 ± 0.03 (98%)	3.43 ± 0.04 (98%)	3.50 ± 0.01 (100%)	
Acetone				
1.50	1.50 ± 0.02 (100%)	1.49 ± 0.03 (100%)	1.41 ± 0.01 (94%)	
2.50	2.49 ± 0.02 (100%)	2.54 ± 0.06 (102%)	2.48 ± 0.04 (99%)	

formula. The robustness of **V** and **VII** against dehydration and rehydration is, therefore, conclusive and can be rationalized by the extraordinary affinity of Ln^{III} for water and the flexible coordination chemistry of Ln^{III}.

The dehydration of **V** (representative of **V** and **VII**) apparently resulted in the aggregates of the shattered crystals (Figure S10) according to inspection using scanning electron microscopy (SEM). Rehydration did not cause any significant changes in the particle size and morphology. Based on the as-described results, dehydration and rehydration are assuredly reversible.

3.4. Robustness of V and VII in Organic Solvents. The robustness of **V** and **VII** in different solvents was also studied. Evidently, the soaking of **V** and **VII** in common organic solvents including ethanol, acetone, acetonitrile, ethyl acetate, THF, dichloromethane, chloroform, benzene, toluene, cyclohexane, and hexane for 24 h did not cause any damage to their crystallinity; therefore, the framework structures of the samples were retained based on the PXRD experiments (Figure 1). The slight broadening and shifting of the most intense (110) diffraction peaks after contact with acetone (**VII**) and acetonitrile (**V** and **VII**) should be noted. This can be indicative of interactions between the two polar solvents and frameworks, although they are very subtle.

3.5. Solid-State Photoluminescence and Colorimetric Properties. The photoluminescence spectra of **I**–**X** and Hdmba at room temperature were first examined in the solid state (Figure 4). Due to the lack of 4f electron in the case of La^{III} (**I**) and the exceptionally high energies of the excited multiplex in the case of Gd^{III} (**VI**), only a broad emission profile of ligand-centered $\pi^* \rightarrow \pi$ emission appeared in their spectra. However, the redshift of the emission from that of Hdmba was apparent. This can be explained by the increased rigidity of the organic ligand upon coordination with Ln^{III} and its interactions with other structural moieties (Tables S3 and S8). The triplet state energy of $dmba^-$ or $T_1(dmba^-)$ was estimated from their spectra to be in the 22,000–23,000 cm^{-1} (435–455 nm) range.

III (Nd^{III}) and **X** (Er^{III}) showed similar $\pi^* \rightarrow \pi$ emissions with maxima at ca. 450 nm. Because sensitization in these frameworks can be reasonably ineffective, the $T_1(dmba^-)$ value of 22,222 cm^{-1} could be calculated. This value is consistent with those estimated for **I** and **VI**. Since $dmba^-$ has been previously reported with only Tb^{III} in $\{[Tb(3,4\text{-dmba})_3(H_2O)_2]\cdot H_2O\cdot C_2H_5OH\}_n$,[29] Pr^{III} in $[Pr(dmba)_3]$,[39] and Ce^{III} in $[Ce(dmba)_3]$,[40] there are no previous data for $T_1(dmba^-)$ for comparison.

Considering the common accepting states of Pr^{III} ($^3P_0$; 20,706 cm^{-1}), Sm^{III} ($^4G_{5/2}$; 17,924 cm^{-1}), Eu^{III} ($^5D_0$; 17,200 cm^{-1}, $^5D_1$; 19,000 cm^{-1}), Tb^{III} ($^5D_4$; 20,500 cm^{-1}), Dy^{III} ($^4F_{9/2}$; 21,144 cm^{-1}), and Ho^{III} ($^5S_2$; 18,354 cm^{-1}, $^5F_3$; 20,673 cm^{-1}), sensitization of **II**, **IV**, **V**, **VII**, **VIII**, and **IX** is feasible. Accordingly, characteristic Pr^{III}: $^3P_J \rightarrow {}^3H_4$ (J = 0–2), Sm^{III}: $^4G_{5/2} \rightarrow {}^6H_J$ (J = 5/2–9/2), Eu^{III}: $^5D_0 \rightarrow {}^7F_J$ (J = 1–4), Tb^{III}: $^5D_4 \rightarrow {}^7F_J$ (J = 6–3), Dy^{III}: $^4F_{9/2} \rightarrow {}^6H_J$ (J = 15/2, 13/2), and Ho^{III}: $^5G_5$, $^3K_8$, $^5F_3 \rightarrow {}^5I_8$ emissions were observed. The emission colors corresponded well with the emission spectra (Figure S11).

The efficiency of energy transfer from the triplet state of $dmba^-$ to the excited states of Ln^{III} or the so-called sensitization, however, varies. The near disappearance of the ligand-centered emissions in the spectra of **V** and **VII** indicates the highly efficient sensitization of Eu^{III} and Tb^{III} by $dmba^-$. The red and green emissions were consistently more vibrant than the other emissions. The measurements of the emission lifetimes revealed a single exponential decay for both red and green emissions (Figure S12). The lifetime of the green emission ($\mathbf{VII}_{as\text{-}syn}$; 0.93(±0.01) ms) was revealed, however, to be longer than the red emission ($\mathbf{V}_{as\text{-}syn}$; 0.62(±0.04) ms). This leads to the conclusion of better Tb^{III} sensitization.[41] Because the local environment of Eu^{III} and Tb^{III} is identical, the environmental quenching effect should, therefore, be less efficient in Tb^{III} than in Eu^{III}.

3.6. Effect of Dehydration and Rehydration on the Emission Spectra and Colors of V and VII. Intrigued by structural robustness as well as intense and vibrant emissions of **V** and **VII**, the effects of dehydration and rehydration on their photoluminescence and colorimetric properties were examined (Figure 5). In contrast to the PXRD results, for which the change in the $\mathbf{VII}_{dehyd}$ structure was substantial, the green

https://doi.org/10.1021/acsomega.4c06958
ACS Omega 2024, 9, 49441–49451

emission was almost unaffected. The red emission of $\mathbf{V}_{dehyd}$ was, on the other hand, completely turned off. The disappeared emission could be, nonetheless, recovered simply and rapidly by soaking in water. The recovery occurred in less than 1 min. However, under ambient air, the recovery process was sluggish.

The turn-off ($\mathbf{V}_{dehyd}$) and turn-on ($\mathbf{V}_{rehyd}$) of the red emission undoubtedly correspond to the absence and presence of water molecules, which are involved immensely in the hydrogen bonding interactions (Table S7). In $\mathbf{V}_{as\text{-}syn}$, the water molecules as well as the methoxy group of $dmba^-$ were transfixed through hydrogen bonding interactions and the suppression of the nonradiative decay can be assumed.[8,27,41−43] The absence of water in $\mathbf{V}_{dehyd}$ would allow $dmba^-$ to move more freely and, thus, the nonradiative decay occurs, which consequently turns off the red emission.[41,43] The restoration of these hydrogen bonding interactions in $\mathbf{V}_{rehyd}$ would restore these interactions and, therefore, the red emission.

The emission lifetimes of $\mathbf{V}_{dehyd}$ and $\mathbf{V}_{rehyd}$ were measured (Figure S12), providing the values of 0.78(±0.05) and 0.68(±0.04) ms, respectively. Considering the intricate fitting of the decay plots and the yielded standard deviations,[41] these values are considered to be similar to that of $\mathbf{V}_{as\text{-}syn}$. These results satisfactorily support our assumption on the crucial role of the competing nonradiative processes and the hydrogen bonding interacions.[8,27,41−43]

3.7. Performance of V as a Selective Colorimetric Probe. To assess the selectivity of $\mathbf{V}_{dehyd}$ toward water, its emission spectra and colors in dried organic solvents, including ethanol, acetonitrile, acetone, ethyl acetate, THF, dichloromethane, chloroform, benzene, toluene, cyclohexane, and hexane, were examined (Figure S13). As expected, the recovery of the Eu^{III} red emission and color could not be effectively induced by organic solvents. Therefore, the turn-on of the red emission is selective only to water, which agrees well with the exceptional affinity of Ln^{III} to water and the molecular sieve property of **V**.

The quantitative correlation between red emission and water content in common organic solvents was studied using $\mathbf{V}_{dehyd}$. The water concentration varied from 0% v/v (dried solvent) to 5% v/v. Noticeably, $\mathbf{V}_{dehyd}$ precipitated in the nonpolar solvents, such as chloroform, hexane, cyclohexane, benzene, and toluene (Figure S14). Precipitation became worse with an increase in water concentration. This incident is not unexpected owing to their opposite polarities. On the other hand, a gradual change in color from black to different shades of red depending on the water concentration was clearly visible in polar solvents (Figure 6).

Inspired by the consistency of the results obtained from several experimental repetitions, the emission colors of the suspensions of $\mathbf{V}_{dehyd}$ in ethanol, acetonitrile, acetone, ethyl acetate, and THF were captured using a smartphone camera. The captured photographs were analyzed using the Color Picker application installed beforehand on the mobile phone.[34] The red (R), blue (B), and luminance (L), which were read out directly from the application, were used to plot against the water concentration (Figures S15−S21). The R and B parameters were presented as the percentage of 255, which represents the purest colorimetric extreme, and the L parameter is a normalized value with respect to white emission (100%).[44]

Satisfactorily, the three most polar solvents, ethanol, acetonitrile, and acetone, provided excellent linear correlations from 0 to 3−5% water content. Excellent R^2 coefficients of >0.98 were obtained. The limits of detection (LODs) and quantification (LOQs) were also calculated. The yielded values are comparable to, if not better than, those of other previously reported colorimetric probes (Table 1). Since many colorimetric parameters can be concurrently employed in the measurements, a cross-check of the measurement results is plausible. This is an advantage of $\mathbf{V}_{dehyd}$ although it can be only used with polar solvents. Notably, the less polar solvents, ethyl acetate, THF, dichloromethane, and chloroform, could not afford such a linear correlation.

The determination of water content in the standard solvent samples was then attempted using the calibration method (Figures 7 and S15−S17 and Table 2). Compared to the expected concentrations and the values determined using the standard Karl Fischer titration in the case of ethanol, the yielded values were exceptional. Reuse of the probe was also demonstrated by using ethanol as the model solvent. The sensing performance remained approximately the same even after five cycles. The framework structure was also retained in accordance with the PXRD experiments and FT-IR spectroscopy (Figures S7 and S22 and Table S14). Nonetheless, the emergence of an additional peak at 2θ of ca. 32° in the PXRD pattern of the reused probe was distinct (Figure S22) from which a slight change in the probe's structure can be assumed. The SEM images of the reused probe did not show any significant changes in the morphology or size of the particles (Figure S10). Therefore, the potential of **V** as a colorimetric probe for the determination of trace water in polar solvents was demonstrated. It should be noted that the use of a mobile phone for determining trace water in organic solvents based on colorimetric analysis is thus far exceptionally few.[34,43−47]

4. CONCLUSIONS

A new series of $[Ln^{III}(dmba)_3(H_2O)_2]\cdot 2H_2O$ (**I**−**X**) were synthesized and characterized. Their structures are composed of one-dimensional $[Ln^{III}(dmba)_3(H_2O)_2]$ chains with a molecular sieve property that allows access only to water. The effects of lanthanide contraction on both the structures and properties were disclosed. The single-crystal structures and Hirshfield analysis indicated extensive hydrogen bonding interactions and their crucial role in transfixing structural components, which consequently promoted emissions from **II**, **IV**, **V**, and **VII**−**IX**. Based on the emissions of **I**, **III**, **VI**, and **X**, $T_1(dmba^-)$ was estimated to span over the 22,000−23,000 cm^{-1} range. The dehydration-induced turn-off and rehydration-induced turn-on of the red emission of **V** were revealed and rationalized by the molecular sieve property of **V**, the exceptional affinity of Ln^{III} (Eu^{III}) for water, and the extensive hydrogen bonding interactions. The excellent potential of $\mathbf{V}_{dehyd}$ as a colorimetric sensing probe for determining trace water in ethanol, acetonitrile, and acetone was demonstrated.

■ ASSOCIATED CONTENT

Supporting Information

The Supporting Information is available free of charge at https://pubs.acs.org/doi/10.1021/acsomega.4c06958.

Details on the materials, instruments, characterization methods, single-crystal structure determination, tables, and figures showing the experimental results. (PDF)

https://doi.org/10.1021/acsomega.4c06958
ACS Omega 2024, 9, 49441−49451

Accession Codes

CCDC 2360645−2360654 contains the supplementary crystallographic data for this paper. These data can be obtained free of charge via www.ccdc.cam.ac.uk/data_request/cif, or by emailing data_request@ccdc.cam.ac.uk, or by contacting The Cambridge Crystallographic Data Centre, 12 Union Road, Cambridge CB2 1EZ, UK; fax: + 44 1223 336033.

AUTHOR INFORMATION

Corresponding Author

Apinpus Rujiwatra − *Department of Chemistry, Faculty of Science, Chiang Mai University, Chiang Mai 50200, Thailand;* orcid.org/0000-0002-2364-4592; Email: apinpus.rujiwatra@cmu.ac.th

Authors

Malee Sinchow − *Office of Research Administration, Chiang Mai University, Chiang Mai 50200, Thailand; Department of Chemistry, Faculty of Science, Chiang Mai University, Chiang Mai 50200, Thailand;* orcid.org/0000-0003-4199-880X

Rania Chaicharoen − *Department of Chemistry, Faculty of Science, Chiang Mai University, Chiang Mai 50200, Thailand*

Thammanoon Chuasaard − *Office of Research Administration, Chiang Mai University, Chiang Mai 50200, Thailand; Department of Chemistry, Faculty of Science, Chiang Mai University, Chiang Mai 50200, Thailand*

Bunlawee Yotnoi − *Department of Chemistry, School of Science, University of Phayao, Phayao 56000, Thailand*

Chalermpong Saenjum − *Department of Pharmaceutical Sciences, Faculty of Pharmacy, Chiang Mai University, Chiang Mai 50200, Thailand*

Athipong Ngamjarurojana − *Department of Physics and Materials Science, Faculty of Science, Chiang Mai University, Chiang Mai 50200, Thailand;* orcid.org/0000-0003-0392-9520

Complete contact information is available at: https://pubs.acs.org/10.1021/acsomega.4c06958

Notes

The authors declare no competing financial interest.

ACKNOWLEDGMENTS

This research was funded by the National Research Council of Thailand (NRCT) and Chiang Mai University (Contract Number N42A670317). M.S. and T.C. thank Chiang Mai University for their support under the CMU Proactive Researcher Scheme.

REFERENCES

(1) Mishra, S.; Singh, A. K. Optical sensors for water and humidity and their further applications. *Coord. Chem. Rev.* **2021**, *445*, No. 214063.

(2) Kumar, P.; Ghosh, A.; Jose, D. A. Chemical sensors for water detection in organic solvents and their applications. *ChemistrySelect* **2021**, *6*, 820−842.

(3) Xu, X.; Li, H.; Xu, Z. Multifunctional luminescent switch based on a porous PL-MOF for sensitivity recognition of HCl, trace water and lead ion. *Chem. Eng. J.* **2022**, *436*, No. 135028.

(4) Parker, D.; Fradgley, J. D.; Wong, K. The design of responsive luminescent lanthanide probes and sensors. *Chem. Soc. Rev.* **2021**, *50*, 8193−8213.

(5) Wang, X.; Chang, H.; Xie, J.; Zhao, B.; Liu, B.; Xu, S.; Pei, W.; Ren, N.; Huang, L.; Huang, W. Recent developments in lanthanide-based luminescent probes. *Coord. Chem. Rev.* **2014**, *273*−*274*, 201−212.

(6) Cui, Y.; Chen, B.; Qian, G. Lanthanide metal-organic frameworks for luminescent sensing and light-emitting applications. *Coord. Chem. Rev.* **2014**, *273*−*274*, 76−86.

(7) Hasegawa, Y.; Kitagawa, Y. Luminescent lanthanide coordination polymers with transformative energy transfer processes for physical and chemical sensing applications. *J. Photochem. Photobiol. C: Photochem. Rev.* **2022**, *51*, No. 100485.

(8) Zhao, X.; Hao, P.; Ling, Y.; Jia, M.; Zhu, R.; Liu, J.; Xu, Q.; Zhou, J. Effects of water molecules on luminescence in europium and terbium coordination polymers with *p*-fluorobenzoic acid as ligand. *J. Rare Earths* **2024**, *42* (7), 1258−1264.

(9) Hefayathullah, M.; Singh, S.; Ganesan, V.; Maduraiveeran, G. Metal-organic frameworks for biomedical applications: A review. *Adv. Colloid Interface Sci.* **2024**, *331*, No. 103210.

(10) Zhao, J.; Zhang, Y.; Luo, Y.; Zheng, W.; Xu, X.; Luo, F. Amorphous metal-organic frameworks: Pioneering frontiers in cancer diagnostics and therapeutics. *Chem. Eng. J.* **2024**, *492*, No. 152295.

(11) Zhang, Z.; Ma, N.; Yao, S.; Han, W.; Li, X.; Chang, H.; Wang, Y. Transparent and hazy Eu_xTb_{1-x}-nanopaper with color-tuning, photo-switching, and white light-emitting properties for anti-counterfeiting and light-softened WLEDs. *ACS Sustainable Chem. Eng.* **2021**, *9* (17), 5827−5837.

(12) Tang, Y.; Wu, H.; Cao, W.; Cui, Y.; Qian, G. Luminescent metal-organic frameworks for white LEDs. *Adv. Opt. Mater.* **2021**, *9* (23), No. 2001817.

(13) Wang, X.; Jiang, Y.; Tissot, A.; Serre, C. Luminescent sensing platforms based on lanthanide metal-organic frameworks: Current strategies and perspectives. *Coord. Chem. Rev.* **2023**, *497*, No. 215454.

(14) Das, R.; Verma, P. K.; Nagaraja, C. M. Design of porphyrin-based frameworks for artificial photosynthesis and environmental remediation: Recent progress and future prospects. *Coord. Chem. Rev.* **2024**, *514*, No. 215944.

(15) Alzard, R. H.; Siddig, L. A.; Abdelhamid, A. S.; Paz, A. P.; Nguyen, H. L.; Sethupathi, K.; Sreejith, P. K.; Alzamly, A. Lanthanide(III) (Er/Ho) coordination polymers for a photocatalytic CO_2 cycloaddition reaction. *Dalton Trans.* **2023**, *52*, 8473−8487.

(16) Biradha, K.; Das, S. K.; Bu, X. H. Coordination polymers as heterogeneous catalysts for water splitting and CO_2 fixation. *Cryst. Growth Des.* **2022**, *22*, 2043−2045.

(17) Das, R.; Ezhil, T.; Palakkai, A. S.; Muthukumar, D.; Pillai, R. S.; Nagaraja, C. M. Efficient chemical fixation of CO_2 from direct air under environment-friendly co-catalyst and solvent-free ambient conditions. *J. Mater. Chem. A* **2021**, *9*, 23127−23139.

(18) Das, R.; Nagaraja, C. M. Noble metal-free Cu(I)-anchored NHC-based MOF for highly recyclable fixation of CO_2 under RT and atmospheric pressure conditions. *Green Chem.* **2021**, *23*, 5195−5204.

(19) Saraci, F.; Quezada-Novoa, V.; Donnarumma, P. R.; Howarth, A. J. Rare-earth metal-organic frameworks: From structure to applications. *Chem. Soc. Rev.* **2020**, *49*, 7949−7977.

(20) You, L.-X.; Ren, B.; He, Y.; Wang, S.; Sun, Y.; Dragutan, V.; Xiong, G.; Ding, F. Structural features of lanthanide coordination polymers with catalytic properties. *J. Mol. Struct.* **2024**, *1304*, No. 137687.

(21) Bünzli, J.-C. Benefiting from the unique properties of lanthanide ions. *Acc. Chem. Res.* **2006**, *39* (1), 53−61.

(22) Wang, X.; Zhang, L.; Yang, J.; Liu, F.; Dai, F.; Wang, R.; Sun, D. Lanthanide metal-organic frameworks containing a novel flexible ligand for luminescence sensing of small organic molecules and selective adsorption. *J. Mater. Chem. A* **2015**, *3*, 12777.

(23) Black, C. A.; Costa, J. S.; Fu, W. T.; Massera, C.; Roubeau, O.; Teat, S. J.; Aromí, G.; Gamez, P.; Reedijk, J. 3-D Lanthanide metal-organic frameworks: Structure, photoluminescence, and magnetism. *Inorg. Chem.* **2009**, *48* (3), 1062−1068.

(24) Zhao, Y.; Liu, J.; Wang, S.; Zhai, X.; Shao, L.; Liu, Y.; Zhang, X.; Chen, J.; Meng, F.; Fu, Y. A dual-emissive europium-based metal-

https://doi.org/10.1021/acsomega.4c06958
ACS Omega 2024, 9, 49441−49451

organic framework for selective and sensitive detection of Fe^{3+} and Fe^{2+}. *Dalton Trans.* **2021**, *50*, 13823−13829.
(25) Hasegawa, M.; Ohmagari, H.; Tanaka, H.; Machida, K. Luminescence of lanthanide complexes: From fundamental to prospective approaches related to water- and molecular-stimuli. *J. Photochem. Photobiol. C: Photochem. Rev.* **2022**, *50*, No. 100484.
(26) Zhang, X.; Jin, X.; Li, Y. Water-induced luminescence improvement in a lanthanide *β*-diketone complex for monitoring water purity. *Chin. Chem. Lett.* **2022**, *33* (4), 2117−2120.
(27) Fan, W.; Cheng, Y.; Feng, M.; Liu, P.; Wang, L.; Liu, Y.; Cao, Q.; Zheng, L. Lanthanide metal-organic framework isomers with novel water-boosting lanthanide luminescence behaviors. *ACS Appl. Mater. Interfaces* **2023**, *15* (35), 41977−41991.
(28) Li, S.-Y.; Yan, X.; Lei, J.; Ji, W.; Fan, S.; Zhang, P.; Zhai, Q. High-performance turn-on fluorescent metal-organic framework for detecting trace water in organic solvents based on the excited-state intramolecular proton transfer mechanism. *ACS Appl. Mater. Interfaces* **2022**, *14* (50), 55997−56006.
(29) Qi, X.-X.; Wu, J.; Ren, N.; Zhao, C.; Zhang, J.; Zong, G.; Gao, J. Novel lanthanide complexes constructed from 3,4-dimethoxybenzoic acid: Crystal structures, spectrum and thermochemical properties. *Thermochim. Acta* **2015**, *615*, 1−7.
(30) *Rikagu Oxford Diffraction, CrysAlisPRO Software System (Version 1.171.39.46)*; Rigaku Corporation: Oxford, U.K., 2018.
(31) Sheldrick, G. M. SHELXT − Integrated space-group and crystal-structure determination. *Acta Crystallogr., Sect. A* **2015**, *71*, 3−8.
(32) Sheldrick, G. M. Crystal structure refinement with SHELXL. *Acta Crystallogr., Sect. C* **2015**, *71*, 3−8.
(33) Dolomanov, O. V.; Bourhis, L. J.; Gildea, R. J.; Howard, J. A.; Puschmann, H. J. OLEX2: A complete structure solution, refinement and analysis program. *J. Appl. Crystallogr.* **2009**, *42*, 339−341.
(34) Zhai, X.; Feng, P.; Song, N.; Zhao, G.; Liu, Q.; Liu, L.; Tang, M.; Tang, Y. Dual-functional ratiometric fluorescent sensor based on mixed-lanthanide metal-organic frameworks for the detection of trace water and temperature. *Inorg. Chem. Front.* **2022**, *9*, 1406−1415.
(35) Williams, D. B. G.; Lawton, M. Drying of organic solvents: Quantitative evaluation of the efficiency of several desiccants. *J. Org. Chem.* **2010**, *75* (24), 8351−8354.
(36) Spek, A. L. Structure validation in chemical crystallography. *Acta Crystallogr., Sect. D* **2009**, *65*, 148−155.
(37) McKinnon, J. J.; Spackman, M. A.; Mitchell, A. S. Novel tools for visualizing and exploring intermolecular interactions in molecular crystals. *Acta Crystallogr., Sect. B* **2004**, *60*, 627−668.
(38) McKinnon, J. J.; Jayatilaka, D.; Spackman, M. A. Towards quantitative analysis of intermolecular interactions with Hirshfeld surfaces. *Chem. Commun.* **2007**, *37*, 3814−3816.
(39) Tenório, K. V.; Teixeira, J. A.; de Campos Pinto, L. M.; Caires, F. J.; Treu-Filho, O.; dos Santos, F. A.; Denck Colman, T. A.; Cuin, A.; Carvalho, C. T. Synthesis and structure of a praseodymium (III) complex with carboxylate ligand: A thermal and spectroscopic study. *J. Rare Earths* **2018**, *36*, 1090−1097.
(40) Tenorio, K. V.; Fortunato, A. B.; Moreira, J. M.; Roman, D.; D'Oliveira, K. A.; Cuin, A.; Brasil, D. M.; Pinto, L. M. C.; Colman, T. A. D.; Carvalho, C. T. Thermal analysis combined with X-ray diffraction/Rietveld method, FT-IR and UV−vis spectroscopy: Structural characterization of the lanthanum and cerium (III) polycrystalline complexes. *Thermochim. Acta* **2020**, *690*, No. 178662.
(41) Thor, W.; Bunzil, J. C. G.; Wong, K. L.; Tanner, P. A. Shedding light on luminescence lifetime measurement and associated data treatment. *Adv. Photonics Res.* **2024**, No. 2400081.
(42) Wang, J.; Jiang, M.; Yan, L.; Peng, R.; Huangfu, M.; Guo, X.; Li, Y.; Wu, P. Multifunctional luminescent Eu(III)-based metal-organic framework for sensing methanol and detection and adsorption of Fe(III) ions in aqueous solution. *Inorg. Chem.* **2016**, *55* (24), 12660−12668.
(43) Manna, P.; Bhar, M.; Mukherjee, P. Lanthanide photoluminescence lifetimes reflect vibrational signature of local environment: Lengthening duration of emission in inorganic nanoparticles. *J. Lumin.* **2021**, *235*, No. 118052.
(44) James, H.; Honeychurch, K. C. Digital image colorimetry smartphone determination of acetaminophen. *J. Chem. Educ.* **2024**, *101* (1), 187−196.
(45) Yu, L.; Zheng, Q.; Xiong, L.; Feng, L.; Xiao, Y. Dual-lanthanide urea metal-organic framework based fluorescent traffic light microsensor for solvent decoding and visual trace water assay. *Sens. Actuators, B* **2022**, *356*, No. 131328.
(46) Zhao, Z.; Hu, Q.; Liu, W.; Xiong, X.; Wang, Z.; Wang, H. A smartphone-available colorimetric and near-infrared fluorescence sensor for trace amounts of water detection in highly polar organic solvents. *Dyes Pigm.* **2023**, *213*, No. 111186.
(47) Wiwasuku, T.; Suebphanpho, J.; Ittisanronnachai, S.; Promarak, V.; Boonmak, J.; Youngme, S. Nanoscale carbon dot-embedded metal-organic framework for turn-on fluorescence detection of water in organic solvents. *RSC Adv.* **2023**, *13*, 18138−18144.

https://doi.org/10.1021/acsomega.4c06958
ACS Omega 2024, 9, 49441−49451